Supporting Information

Application of heterojunction Ni-Sb-SnO_2 anodes for electrochemical water treatment

Yi Zhang,[1#] Yang Yang,[1,2#] Shasha Yang,[2] Estefanny Quispe-Cardenas,[2] Michael R. Hoffmann[1*]

1. Linde Laboratories, California Institute of Technology, Pasadena, CA 91125

2. Department of Civil and Environmental Engineering, Clarkson University, NY 13699

# These authors contribute equally

Text S1. Analytical methods.

Benzoic acid (BA), nitrobenzene (NB), and phenol (Ph) were quantified by high-performance liquid chromatography (HPLC) equipped with an XDB-Phenyl column (Agilent, 2.1 × 50 mm, 5 µm particles) at 226 and 250 nm. The eluent had a flow rate of 0.5 mL/min and consisted of 10% acetonitrile (ACN) and 90% water with 0.1% formic acid.

Pharmaceutical degradation was analyzed using HPLC with an XDB-C18 column (Agilent, 2.1 × 50 mm, 3.5 µm particles), the eluent flowed at 0.5 mL/min and consisted of ACN and water with 0.1% formic acid. A gradient was used to resolve peaks: 0 min, 5% ACN; 0.6 min, 5% ACN; 9.6 min, 95% ACN; 10.5 min, 95% ACN; 10.8 min, 5% ACN; 15 min, 5% ACN.

Model compound degradation and transformation products were identified using an ultrahigh performance liquid chromatography system (Waters Acquity UPLC) with an Acquity BEH C18 column (2.1 × 50 mm, 1.7 µm particles) coupled to a time-of-flight mass spectrometer (Waters Xevo GS-2 TOF). Eluent consisting of ACN and water with 0.1% formic acid flowed at 0.5 mL/min. The gradient was: 0 min, 5% ACN; 0.2 min, 5% ACN; 3.2 min, 95% ACN; 3.5 min, 95% ACN; 3.6 min, 5% ACN; 5 min, 5% ACN. Conditions used for mass spectrometer were: ibuprofen (IBP) – negative electrospray ionization (ESI-) in resolution mode, capillary voltage 1.0 kV; carbamazepine (CBZ) – positive electrospray ionization (ESI+) in resolution mode, capillary voltage 0.2 kV. Cone voltage 50 V, source offset 80 V, source temperature 120°C, desolvation temperature 400°C, cone gas 40 L/h, desolvation gas 800 L/h, 0.3 s scan time in continuum mode, collision energy 1.0 eV, and second acquisition channel collision energy scanned from 0 to 30 eV. A leucine lock-mass was used to correct for accurate mass values.

Trihalomethanes (THMs) and haloacetic acids (HAAs) were extracted using a previously reported method.[1] Briefly, THMs were extracted in pentane and collected after centrifugation

(5000 rpm, 5 min). HAAs (1 mL water sample) were extracted in 2 mL methyl tert-butyl ether (MTBE) following adjustment of pH (0.1 mL concentrated sulfuric acid) and ionic strength (0.5 g sodium sulfate). Sample methylation was completed with acidic methanol (1 mL 10% sulfuric acid in methanol) at 50℃ for 2 hours. Formed HAA-esters were cleaned using 10% sodium sulfate in water (4 mL), and the upper ether layer was collected for analysis.

THMs and HAAs extracts were analyzed by gas chromatography equipped with an electron capture detector (GC/ECD, Agilent 7890). Helium was used as a detector makeup gas in constant makeup mode at 30 mL/min. Separation was performed on a 30 m Rxi-5ms column (0.25 mm i.d., 0.25 µm film thickness, RESTEK). Helium was used as the carrier gas in constant flow mode at 1 mL/min. For THMs, the oven was initially set to 30℃ (hold for 2 min), then programmed as follows: 5℃/min to 50℃ (hold for 2 min), 35℃/min to 150℃ (hold for 5 min), then 25℃/min to 185℃ (hold for 5 min). For HAAs, the oven was initially set to 40℃ (hold for 10 min), then programmed as follows: 2.5℃/min to 65℃, 10℃/min to 85℃, then 20℃/min to 205℃ (hold for 7 min). The injector temperature was set to 200℃ for both methods.

Metal leaching (Sb, Ni, Sn, Ti) from anodes was analyzed by an Inductively Coupled Plasma Mass Spectrometry (Thermo Scientific, iCAP™ RQ ICP-MS). Samples were first aerosolized by a nebulizer and then introduced into a radiofrequency Argon plasma, causing atomization and ionization to be separated based on their mass-to-charge ratio (m/z ratio) by a single quadrupole mass spectrometer. Experiments were performed using acid-washed and air-dried glass beakers (nitric acid optima grade) using 40 mL NaClO4 (100 mM) as the electrolyte solution with a current density of 10 mA/cm^2. The solution was mixed continuously during the EC experiment using clean magnetic stirrers (experiment time 90 min), and samples were collected using acid-washed pipette tips and microcentrifuge tubes (using 10% nitric acid). Samples were diluted using 2% optima-

grade nitric acid and spiked with 1 mg/L internal standard (Yttrium, Scandium, and Cerium) for quality assurance and quality control (QA/QC). The lower limit of quantification (LOQ) was 10 ng/L based on the background levels of the compounds. Calibration standards and instrument and method blanks (2% nitric acid and Milli-Q water used to prepare electrolyte, respectively) were injected to validate experimental conditions and determine background levels. Finally, a standard was reinjected during the sequence to validate the instrument response. A calibration curve with an $R^2 > 0.9998$ was used to determine the metal concentrations in all replicates.

Text S2. Kinetic modeling.

Kinetic modeling was performed using the chemical kinetics software Kintecus 6.80.[2] A total of 102 elementary reactions were included in the model. pH was set to 2 in all fitting scenarios. Rate constants were obtained from literature or calibrated from experimental and fitting results. The reactions implemented in the model were provided in Table S2.

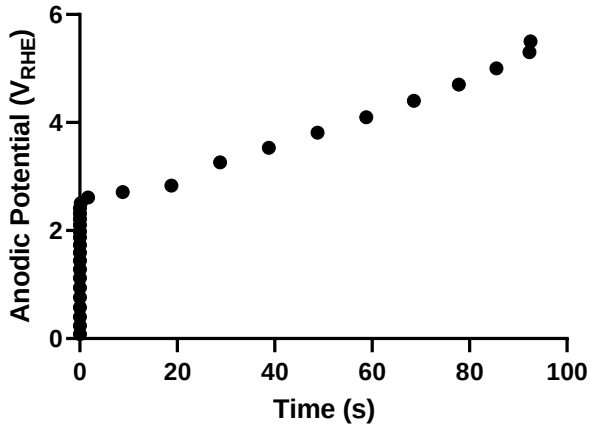

Figure S1. Stability test of Ni (1 atom-%)-SnO_2 electrode at 10 mA/cm^2 in 100 mM $NaClO_4$.

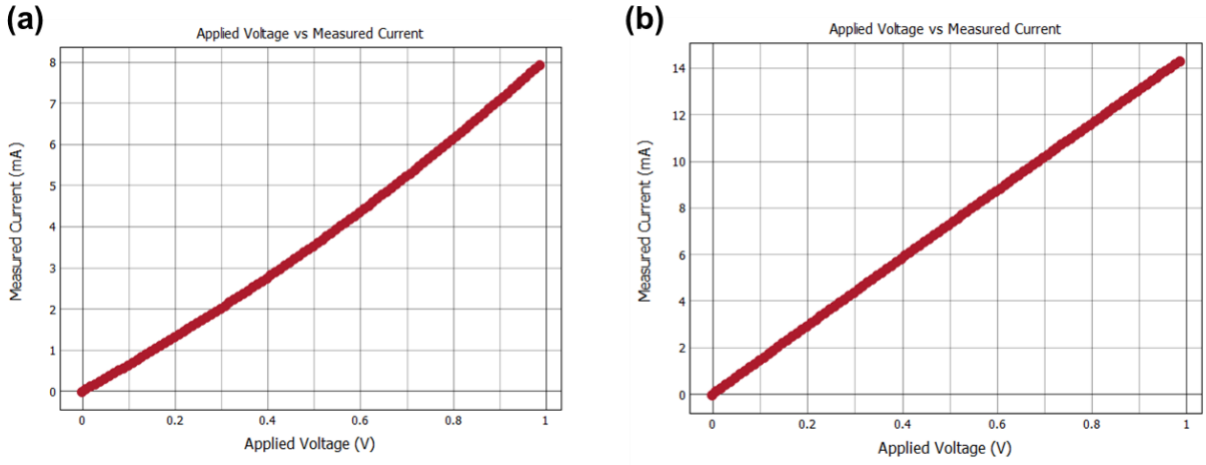

Figure S2. Sheet resistance measurements of (a) NAT and (b) AT.

The tests were performed on an Ossila® four-point probe. NAT and AT have much lower sheet resistance than the indium-tin-oxide glass standard sample (17 ohm/square provided by Ossila®). They are both considered as metallic conductive with no specific sheet resistance given. Comparing the slopes of current-voltage curves of the outer forced connections gives a qualitative conclusion that NAT has a conductivity similar to AT.

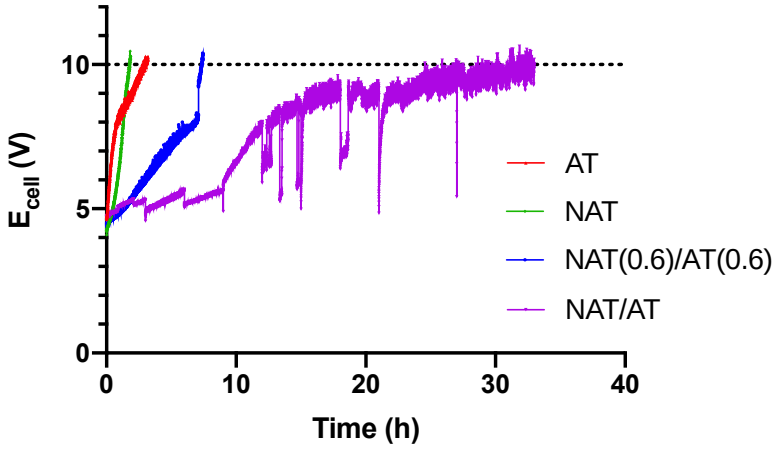

Figure S3. Accelerated lifetime tests of electrodes.

In the accelerated lifetime tests, anodes with a surface area of 0.5 cm^2 were subjected to 100 mA current (current density 200 mA/cm^2). Deactivation is reflected in the cell voltage (E_{cell}) vs. time plot by the increase of E_{cell} to above 10 V, at which point the titanium metal base starts to be corroded.[35] The actual lifetime (t_{oc}) of an electrode at a specific operating current (I_{oc}) can be estimated using the lifetime (t_{alt}) under high current (I_{alt}) based on the empirical equation[3,4]:

$$t_{oc} = \frac{I_{alt}^{1.7} t_{alt}}{I_{oc}^{1.7}}$$

Lifetimes under high current for AT, NAT, and NAT/AT were 2.1, 1.6, and 33 h, which correspond to lifetimes at 10 mA/cm^2 as 342, 260, and 5373 h, respectively. Lifetime for NAT(0.6)/AT(0.6) at 10 mA/cm^2 was calculated to be 1156 h.

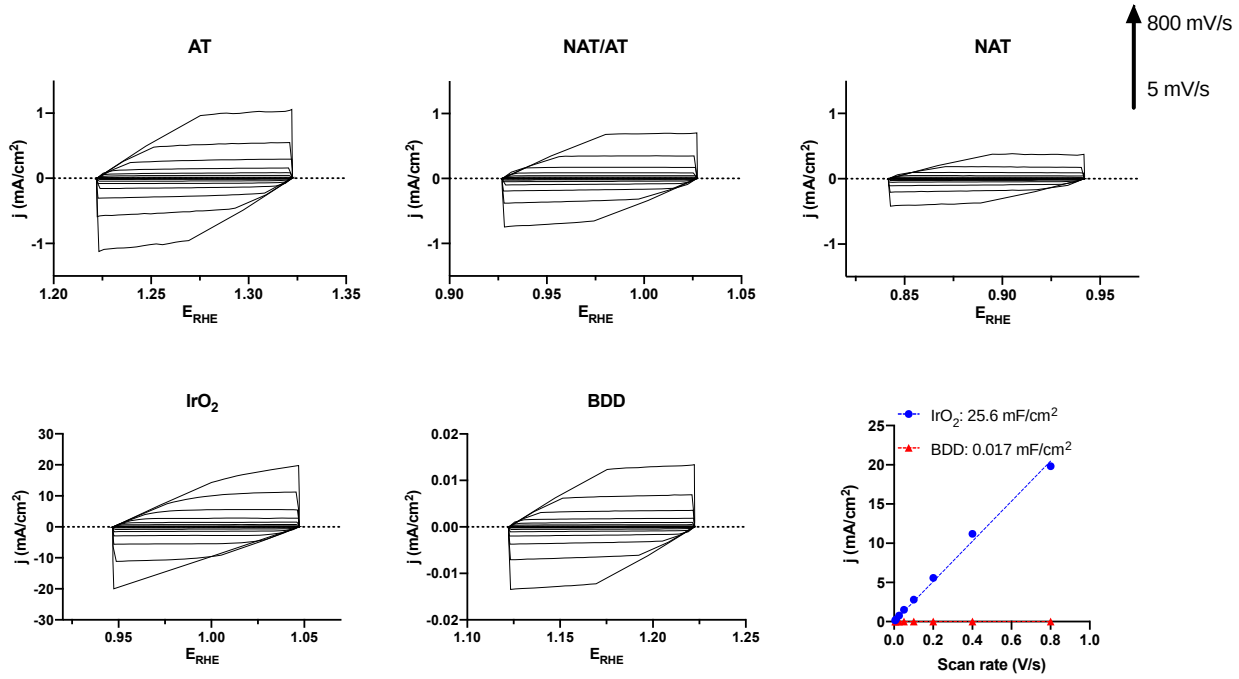

Figure S4. Cyclic voltammograms at scan rates of 5, 10, 25, 50, 100, 200, 400, and 800 mV/s of AT, NAT/AT, NAT, IrO_2, and BDD electrodes and charging currents as functions of scan rate of IrO_2 and BDD electrodes.

The slopes of the charging curves give capacitances (mF/cm^2) that are proportional to the ECSA. Multiplying by the electrode geometric area (6 cm^2) and dividing by a general specific capacitance for metal oxide (0.04 mF/cm^2) gave ECSA values for AT, NAT/AT, NAT, IrO_2, and BDD of 201, 130, 70, 3840, and 2.5 cm^2, respectively. The commercial IrO_2 anode demonstrated a very large ECSA. The reason is unclear due to the proprietary manufacturing procedure. Possibly explanation lies in the porous structure and high mass loading of catalyst (10 mg/cm^2 according to the supplier). On the other hand, BDD had a smaller ECSA than its geometric surface area (2.5 vs. 6 cm^2), likely due to the heterogeneous distribution of electro-active sites on the BDD surface. Not all the crystal facets of BDD have activity towards redox couples used in the ECSA measurement.[5]

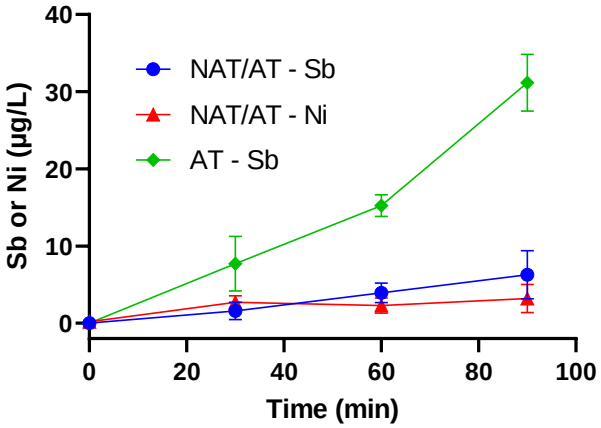

Figure S5. Leaching of Sb and Ni by AT and NAT/AT electrodes.

All electrodes were subjected to 90 min aging at 10 mA/cm^2 before the leaching tests. The 90 min leaching tests were performed three times for each electrode. Fresh electrolyte (100 mM $NaClO_4$) was used in each run. Averages of triplicate experiments are shown. Error bars represent standard deviations.

Based on the precursor composition and the average mass loading of 1.3 mg/cm^2 of the layer exposed to the electrolyte, the total mass of Sb in the form of Sb_2O_3 are 378 and 757 µg for NAT/AT and AT, respectively. A 90 min electrolysis tested by AT released 31 µg/L of Sb in 25 mL electrolyte, equivalent to 0.93 µg Sb_2O_3. This accounts for 0.1% loss of the total Sb_2O_3 from the AT electrode. Similarly, the leaching test indicates that NAT/AT lost 0.05% of the total Sb_2O_3 after 90 min electrolysis.

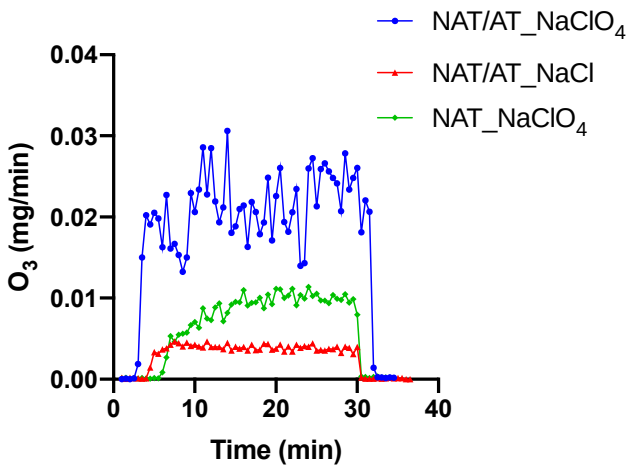

Figure S6. Evolution rates of O_3 in the gas phase during electrolysis in $NaClO_4$ and NaCl electrolytes. Anode surface area = 6 cm^2, current density = 10 mA/cm^2, electrolyte volume = 25 mL.

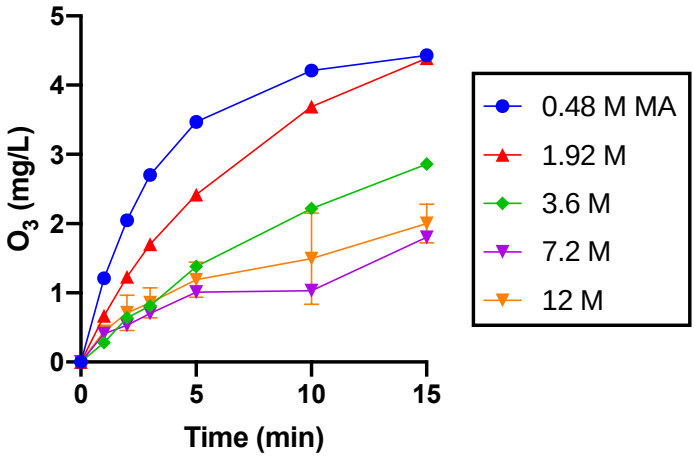

Figure S7. Apparent O_3 production with different concentrations of malonic acid (MA) added to quench free chlorine. Anode surface area = 6 cm^2, current density = 10 mA/cm^2, electrolyte volume = 25 mL.

The result for O_3 production contradicts that from a previous study on Ni-Sb-SnO_2, which reported enhanced ozone production in the presence of Cl^-.[6] The authors likely arrived at their conclusion because the amount of malonic acid (MA) added was insufficient to mask chlorine. During electrolysis, when a small amount of MA (0.48 M) was added, O_3 appeared to be produced faster due to decolorization caused by unmasked chlorine species. However, with increased MA concentrations, the rate of O3 generation inferred by decolorization of potassium indigo trisulfonate decreased and gradually approached a specific level that is slower compared to electrolysis in $NaClO_4$ solution.

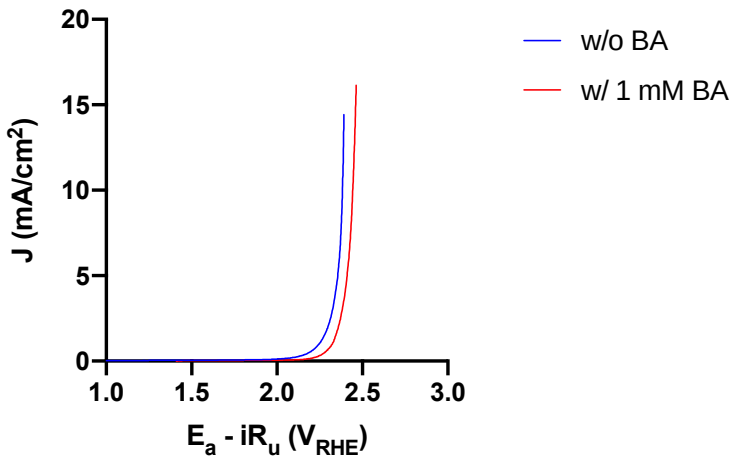

Figure S8. Linear sweep voltammograms (LSV) of NAT/AT in 30 mM $NaClO_4$ electrolytes in the absence and presence of 1 mM benzoic acid (BA).

Direct electron transfer (DET) to the electrode would be indicated by a redox peak in the presence of BA. Such signal was not observed on NAT/AT, thus ruling out the contribution to BA degradation by DET.

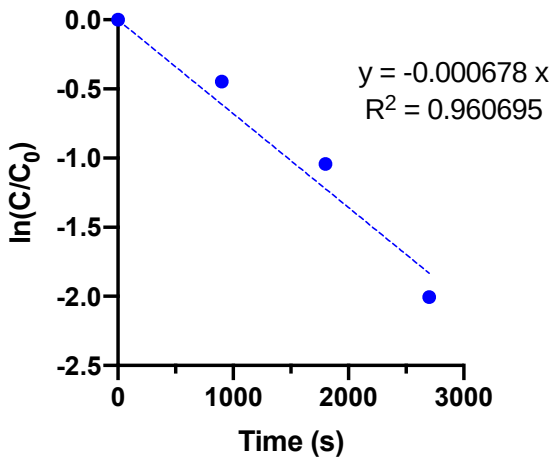

Figure S9. BA degradation by NAT/AT in 30 mM $NaClO_4$ electrolytes.

Assuming that BA degradation follows pseudo first-order kinetics, the fitted rate constant was k_{BA} = 0.000678 s^{-1}, which, normalized by the specific surface area (24 m^2/m^3), is $k_{BA,SA}$ = 2.83 × 10^{-5} m/s.

The steady-state concentration of ·OH ($[\cdot OH]_{ss}$) can be estimated using k_{BA}:

$$\frac{d[BA]}{dt} = k_{BA,OH}[BA][\cdot OH]_{ss} = k_{BA}[BA]$$

$$[\cdot OH]_{ss} = \frac{k_{BA}}{k_{BA,OH}} = 1.58 \times 10^{-13}\ M$$

where k_{BA} is the pseudo-first-order rate constant and $k_{BA,OH}$ is the second-order rate constant for BA and ·OH. The number matches that predicted by the kinetic model, which is ~1.6 × 10^{-13} M in $NaClO_4$ solutions.

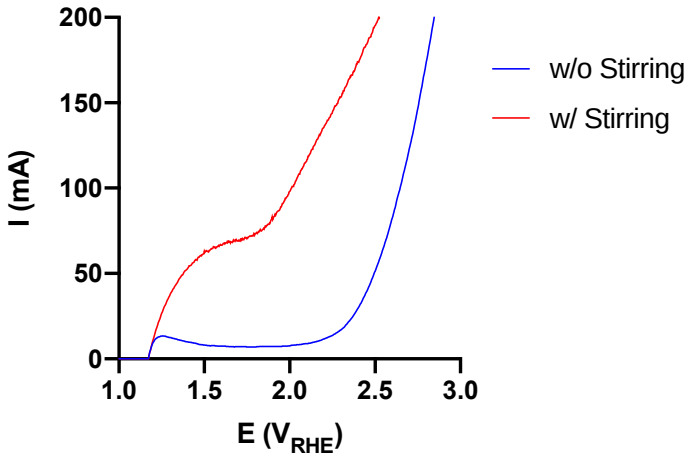

Figure S10. Experimental current vs. applied potential of NAT/AT with and without stirring.

The experiment was measured in 0.5 M Na_2CO_3, 0.05 M $K_4Fe(CN)_6$, and 0.1 M $K_3Fe(CN)_6$. The limiting currents (I_{lim}) with and without stirring were ~70 and 7 mA, respectively. The mass transfer rate constants (k_m) can then be calculated[7]:

$$k_m = \frac{I_{lim}}{nFAC} = \frac{0.07\ \text{A or } 0.007\ \text{A}}{1(96485 \times 1000\ \text{C/kmol})(0.0006\ \text{m}^2)(0.05\ \text{kmol/m}^3)}$$

$$= 2.42 \times 10^{-5}\ \text{m/s or } 2.42 \times 10^{-6}\ \text{m/s}$$

where I_{lim} is the limiting current (plateau region), n is the number of electrons exchanged, F is Faraday constant (96,485 C/mol), A is the electrode surface area, and C is the concentration of the compound of interest in the bulk solution.

Knowing the diffusion coefficient for $Fe(CN)_6^{4-}$ D = 6.58×10^{-10} m^2/s,[8] the diffusion layer thickness (δ) can be calculated:

$$\delta = \frac{D}{k_m} = \frac{6.58 \times 10^{-10}\ \text{m}^2/\text{s}}{0.0000242\ \text{m/s or } 0.00000242\ \text{m/s}} = 2.72 \times 10^{-5}\ \text{m or } 2.72 \times 10^{-4}\ \text{m}$$

that is, the diffusion layer thickness (δ) is ~27 µm (with stirring) or ~270 µm (without stirring).

Assuming the same diffusion layer thickness (δ) for benzoic acid (BA) systems and knowing the diffusion coefficient D_{BA} = 0.9 × 10^{-9} m^2/s for BA at 25°C,[9] a more accurate mass transfer rate constant for BA ($k_{m,BA}$) can be estimated as follows:

$$k_{m,BA} = \frac{D_{BA}}{\delta} = \frac{0.9 \times 10^{-9} m^2/s}{2.72 \times 10^{-5}\ m} = 3.31 \times 10^{-5}\ m/s$$

The limiting current (assuming mineralization of BA) in this system initially can then be estimated:

$$I_{lim,BA} = nFAk_{m,BA}C_{BA} = (4x + y - 2z)FAk_{m,BA}C_{BA}$$

$$= (28 + 6 - 4)(96485 \times 1000\ C/kmol)(0.0006\ m^2)(3.31 \times 10^{-5}\ m/s)(0.001\ kmol/m^3)$$

$$= 0.057\ A$$

where x, y, and z are the number of C, H, and O in BA ($C_7H_6O_2$), respectively. $I_{lim,BA}$ drops during treatment as C_{BA} drops. BA degradation is under mass transport control during the course of electrolysis.

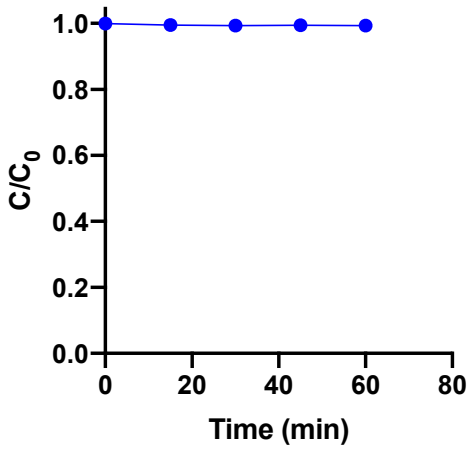

Figure S11. Benzoic acid (BA) degradation by homogeneous ozonation.

In order to exclude the contribution to BA degradation by the direct reaction between O_3 and BA and to mimic the produced O_3 concentration in actual electrolysis experiments, O_3 in the headspace of the electrolysis cell using NAT/AT in 100 mM $NaClO_4$ electrolyte (~40% of total O_3 generated) was purged by N_2 gas into another beaker containing 1 mM BA solution. No BA removal was observed during one-hour electrolysis, confirming our hypothesis that direct reaction between O_3 and BA did not contribute to BA degradation.

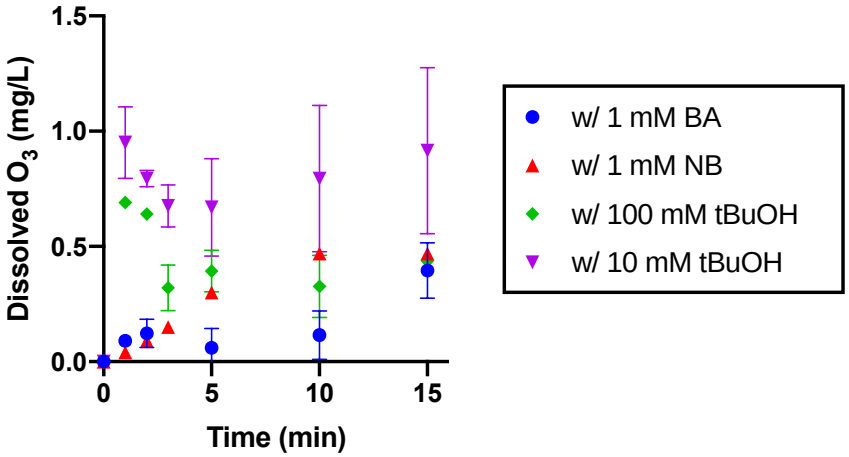

Figure S12. Impacts of the organic radical quenchers benzoic acid (BA), nitrobenzene (NB), and tert-butanol (tBuOH) on the production of O_3 by NAT/AT in 30 mM $NaClO_4$ electrolytes. Anode surface area = 6 cm^2, current density = 10 mA/cm^2, electrolyte volume = 25 mL.

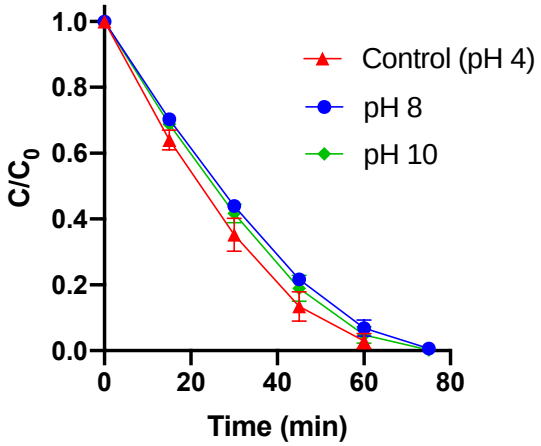

Figure S13. Effect of pH on BA degradation kinetics by NAT/AT. Anode surface area = 6 cm^2, current density = 10 mA/cm^2, electrolyte volume = 25 mL.

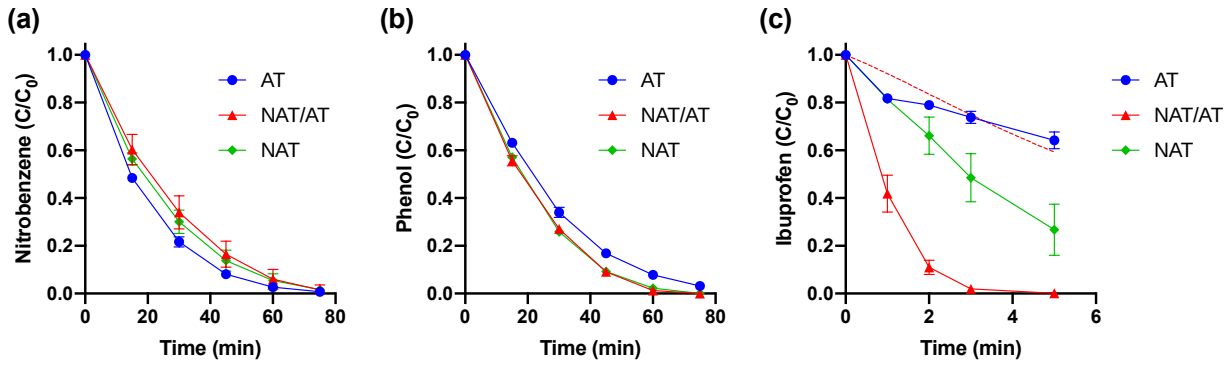

Figure S14. EO treatment of (a) nitrobenzene (NB), (b) phenol (Ph), and (c) ibuprofen (IBP) in 30 mM $NaClO_4$ electrolytes. The dashed red line in (c) represents kinetic model prediction of IBP degradation, taking into account reactions with both O_3 and ·OH. Anode surface area = 6 cm^2, current density = 10 mA/cm^2, electrolyte volume = 25 mL.

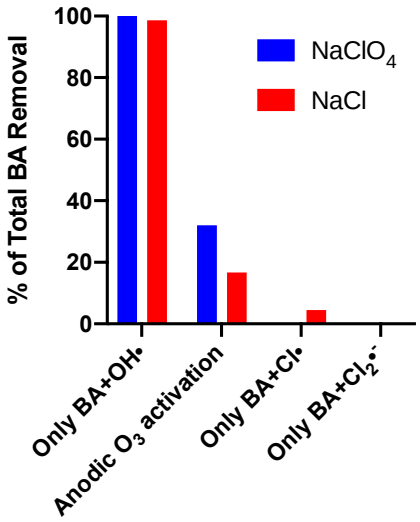

Figure S15. Radical contributions to BA degradation by NAT/AT in 30 mM $NaClO_4$ and NaCl electrolytes.

The model predicted that total BA removal in $NaClO_4$ and NaCl electrolytes at 1 h were ~94% and 76%, respectively. Contributions from specific radical species were quantified by turning on only its reaction with BA and excluding the others. In both electrolytes, contributions from $O^{\cdot -}$ were negligible (no BA removal was predicted with only BA + $O^{\cdot -}$) and thus not shown. Inside the contribution from ·OH, by turning on/off electrochemical ·OH production (reaction 10 in Table S2), sub-contributions from anodic O_3 activation were estimated to be ~32% and 17%, respectively, in $NaClO_4$ and NaCl electrolytes. Contributions from $Cl^{\cdot}$ and $Cl_2^{\cdot -}$ in NaCl were not important, responsible for <5% and <<1% of total removal, respectively.

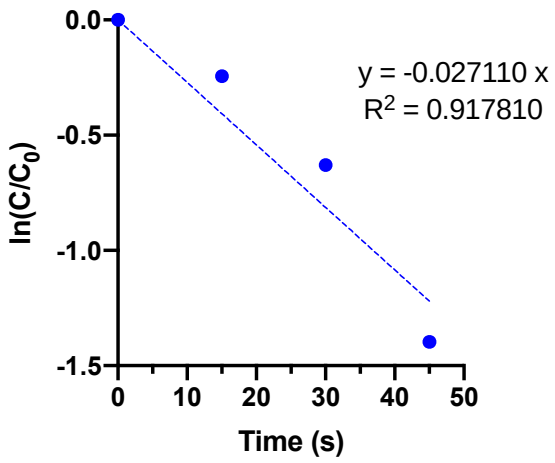

Figure S16. Carbamazepine (CBZ) degradation by NAT/AT in 30 mM $NaClO_4$ electrolytes.

Assuming that CBZ degradation follows pseudo-first-order kinetics, the fitted rate constant was k_{CBZ} = 0.027110 s^{-1}, which, normalized by the specific surface area (24 m^2/m^3), is $k_{CBZ,SA}$ = 1.13 × 10^{-3} m/s. Comparing to that for BA, this assumption is less accurate due to the reaction between CBZ and O_3 in the aqueous phase, which is also manifested in the rate constant that is two orders of magnitude higher than the mass transfer rate constants.

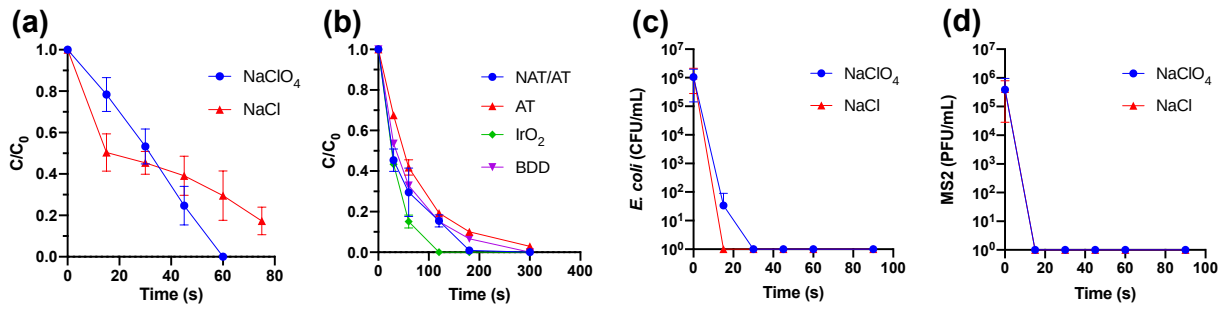

Figure S17. Removal of 30 µM carbamazepine (CBZ) by (a) NAT/AT in 30 mM $NaClO_4$ and NaCl and (b) different electrodes in 30 mM NaCl electrolytes. Inactivation of (c) *E. coli* and (d) MS2 by NAT/AT in 30 mM $NaClO_4$ and NaCl electrolytes. Anode surface area = 6 cm^2, current density = 10 mA/cm^2, electrolyte volume = 25 mL.

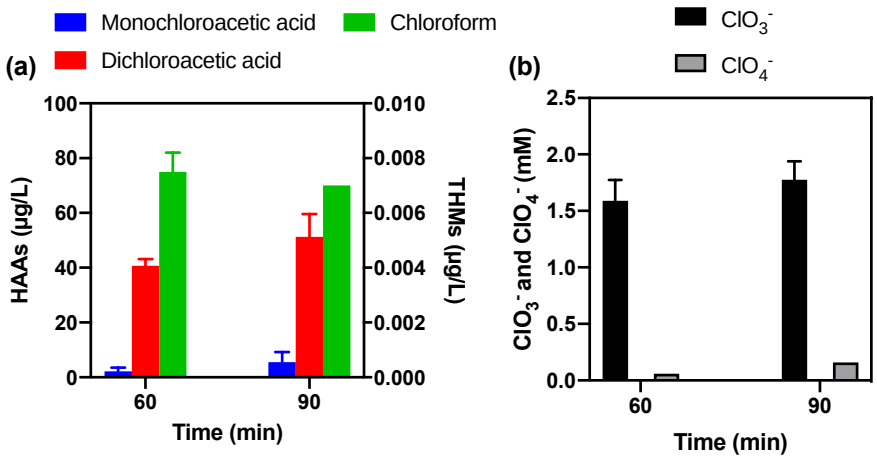

Figure S18. Formation of disinfection byproducts (DBPs) by NAT/AT during electrolysis of latrine wastewater.

Table S1. Target compound properties.

Compound	Hammett constant (σ)[a]	$k_{\cdot OH}$ ($M^{-1}s^{-1}$)	$logK_{ow}$[b]	pKa	Reference
Benzoic acid (BA)	-	4.3×10^9	1.89	4.19	[10]
Nitrobenzene (NB)	0.78 ($-NO_2$)	3.9×10^9	1.85	n.a.	[10]
Phenol (Ph)	-0.36 (-OH)	6.6×10^9	1.44	9.95	[10]
Ibuprofen (IBP)	-	7.2×10^9	2.48-3.97	5.3	[11]

a. NB has an electron-withdrawing ring substituent with a Hammett constant of $\sigma = 0.78$, while the hydroxyl group on Ph has a $\sigma = -0.36$, yet either compound was promoted by anodic O_3 activation, suggesting there is no clear correlation between electron-withdrawing/donating capacity of the ring substituent and activation.
b. BA and NB share really close $logK_{ow}$, but one was promoted and the other was not, indicating there is no clear correlation between $logK_{ow}$ and activation.

Table S2. Principle reactions in the kinetic model.

No.	Reaction	Rate constant	Reference
1	$H^+ + OH^- \rightarrow H_2O$	1.00×10^{11} $M^{-1}s^{-1}$	[12]
2	$H_2O \rightarrow H^+ + OH^-$	1.00×10^{-3} s^{-1}	[12]
3	$H^+ + HO_2^- \rightarrow H_2O_2$	5.00×10^{10} $M^{-1}s^{-1}$	[12]
4	$H_2O_2 \rightarrow H^+ + HO_2^-$	1.30×10^{-1} s^{-1}	[12]
5	$H^+ + Cl^- \rightarrow HCl$	5.00×10^{10} $M^{-1}s^{-1}$	[12]
6	$HCl \rightarrow H^+ + Cl^-$	8.60×10^{16} s^{-1}	[12]
7	$H^+ + OCl^- \rightarrow HOCl$	5.00×10^{10} $M^{-1}s^{-1}$	[12]
8	$HOCl \rightarrow H^+ + OCl^-$	1.40×10^{3} s^{-1}	[12]
9	$MO \rightarrow O_3$	$6.92/1.42 \times 10^{-7}$ s^{-1}	Fitted[a]
10	$MO \rightarrow HO\cdot$	1.69×10^{-6} s^{-1}	Fitted
11	$MO + Cl^- \rightarrow Cl\cdot$	1.50×10^{-5} s^{-1}	Fitted
12	$MO + 2Cl^- \rightarrow Cl_2$	8.05×10^{-1} s^{-1}	Fitted
13	$MO + OCl^- \rightarrow OCl\cdot$	3.89×10^{2} s^{-1}	Fitted

14	$MO + OCl^- \rightarrow ClO_3^-$	Not important[b]	
15	$MO + ClO_3^- \rightarrow ClO_4^-$	Not important[b]	
16	$HO\cdot + H_2O_2 \rightarrow HO_2\cdot + H_2O$	$2.70 \times 10^7\ M^{-1}s^{-1}$	[10]
17	$HO\cdot + OH^- \rightarrow O\cdot^- + H_2O$	$1.20 \times 10^{10}\ M^{-1}s^{-1}$	[13]
18	$HO\cdot + HO\cdot \rightarrow H_2O_2$	$5.50 \times 10^9\ M^{-1}s^{-1}$	[10]
19	$HO\cdot + Cl^- \rightarrow ClOH\cdot^-$	$4.30 \times 10^9\ M^{-1}s^{-1}$	[14]
20	$HO\cdot \rightarrow$ Products	$1.00 \times 10^7\ s^{-1}$	Assumed[c]
21	$ClOH\cdot^- \rightarrow Cl^- + HO\cdot$	$6.10 \times 10^9\ s^{-1}$	[14]
22	$ClOH\cdot^- + H^+ \rightarrow Cl\cdot + H_2O$	$2.10 \times 10^{10}\ M^{-1}s^{-1}$	[14]
23	$ClOH\cdot^- + Cl^- \rightarrow Cl_2\cdot^- + OH^-$	$1.00 \times 10^4\ M^{-1}s^{-1}$	[15]
24	$Cl\cdot + H_2O \rightarrow ClOH\cdot^- + H^+$	$2.50 \times 10^5\ M^{-1}s^{-1}$	[16]
25	$Cl\cdot + H_2O_2 \rightarrow HO_2\cdot + Cl^- + H^+$	$2.00 \times 10^9\ M^{-1}s^{-1}$	[17]
26	$Cl\cdot + OH^- \rightarrow ClOH\cdot^-$	$1.80 \times 10^{10}\ M^{-1}s^{-1}$	[18]
27	$Cl\cdot + Cl^- \rightarrow Cl_2\cdot^-$	$8.00 \times 10^9\ M^{-1}s^{-1}$	[19]
28	$Cl_2\cdot^- + H_2O \rightarrow Cl^- + HClOH$	$1.30 \times 10^3\ M^{-1}s^{-1}$	[16]
29	$Cl_2\cdot^- + H_2O_2 \rightarrow HO_2\cdot + 2Cl^- + H^+$	$1.40 \times 10^5\ M^{-1}s^{-1}$	[20]
30	$Cl_2\cdot^- + OH^- \rightarrow ClOH\cdot^- + Cl^-$	$4.50 \times 10^7\ M^{-1}s^{-1}$	[15]
31	$Cl_2\cdot^- \rightarrow Cl\cdot + Cl^-$	$6.00 \times 10^4\ s^{-1}$	[19]
32	$HClOH \rightarrow Cl\cdot + H_2O$	$1.00 \times 10^2\ s^{-1}$	[16]
33	$HClOH \rightarrow ClOH\cdot^- + H^+$	$1.00 \times 10^8\ s^{-1}$	[16]
34	$HClOH + Cl^- \rightarrow Cl_2\cdot^- + H_2O$	$5.00 \times 10^9\ M^{-1}s^{-1}$	[16]
35	$Cl\cdot + Cl\cdot \rightarrow Cl_2$	$8.80 \times 10^7\ M^{-1}s^{-1}$	[21]
36	$Cl\cdot + Cl_2\cdot^- \rightarrow Cl^- + Cl_2$	$2.10 \times 10^9\ M^{-1}s^{-1}$	[17]
37	$Cl_2\cdot^- + HO\cdot \rightarrow HOCl + Cl^-$	$1.00 \times 10^9\ M^{-1}s^{-1}$	[22]
38	$Cl_2\cdot^- + Cl_2\cdot^- \rightarrow 2Cl^- + Cl_2$	$9.00 \times 10^8\ M^{-1}s^{-1}$	[17]

39	$Cl_2 + H_2O \rightarrow HOCl + Cl^- + H^+$	$1.50 \times 10^1\ M^{-1}s^{-1}$	[23]
40	$Cl_2 + H_2O_2 \rightarrow O_2 + 2HCl$	$1.30 \times 10^4\ M^{-1}s^{-1}$	[20]
41	$Cl_2 + O_2^{\cdot -} \rightarrow O_2 + Cl_2^{\cdot -}$	$1.00 \times 10^9\ M^{-1}s^{-1}$	[20]
42	$Cl_2 + HO_2^{\cdot} \rightarrow O_2 + Cl_2^{\cdot -} + H^+$	$1.00 \times 10^9\ M^{-1}s^{-1}$	[24]
43	$Cl_2 + Cl^- \rightarrow Cl_3^-$	$2.00 \times 10^4\ M^{-1}s^{-1}$	[25]
44	$Cl_3^- + O_2^{\cdot -} \rightarrow Cl_2^{\cdot -} + Cl^- + O_2$	$3.80 \times 10^9\ M^{-1}s^{-1}$	[20]
45	$Cl_3^- + HO_2^{\cdot} \rightarrow Cl_2^{\cdot -} + HCl + O_2$	$1.00 \times 10^9\ M^{-1}s^{-1}$	[24]
46	$Cl_3^- \rightarrow Cl_2 + Cl^-$	$1.10 \times 10^5\ s^{-1}$	[25]
47	$HOCl + H_2O_2 \rightarrow HCl + H_2O + O_2$	$1.10 \times 10^4\ M^{-1}s^{-1}$	[26]
48	$HOCl + HO^{\cdot} \rightarrow OCl^{\cdot} + H_2O$	$2.00 \times 10^9\ M^{-1}s^{-1}$	[20]
49	$HOCl + O_2^{\cdot -} \rightarrow Cl^{\cdot} + OH^- + O_2$	$7.50 \times 10^6\ M^{-1}s^{-1}$	[20]
50	$HOCl + HO_2^{\cdot} \rightarrow Cl^{\cdot} + H_2O + O_2$	$7.50 \times 10^6\ M^{-1}s^{-1}$	[20]
51	$HOCl + Cl^{\cdot} \rightarrow OCl^{\cdot} + Cl^- + H^+$	$3.00 \times 10^9\ M^{-1}s^{-1}$	[18]
52	$HOCl + Cl^- + H^+ \rightarrow Cl_2 + H_2O$	$1.82 \times 10^4\ M^{-2}s^{-1}$	[23]
53	$OCl^- + H_2O_2 \rightarrow Cl^- + H_2O + O_2$	$1.70 \times 10^5\ M^{-1}s^{-1}$	[26]
54	$OCl^- + HO^{\cdot} \rightarrow OCl^{\cdot} + OH^-$	$8.80 \times 10^9\ M^{-1}s^{-1}$	[20]
55	$OCl^- + O_2^{\cdot -} + H_2O \rightarrow Cl^{\cdot} + 2OH^- + O_2$	$2.00 \times 10^8\ M^{-2}s^{-1}$	[20]
56	$OCl^- + Cl^{\cdot} \rightarrow OCl^{\cdot} + Cl^- + H^+$	$8.20 \times 10^9\ M^{-1}s^{-1}$	[18]
57	$OCl^{\cdot} + OCl^{\cdot} \rightarrow P3$	$7.50 \times 10^9\ M^{-1}s^{-1}$	[27]
58	$O_3 + H_2O_2 \rightarrow O_2 + HO^{\cdot} + HO_2^{\cdot}$	$6.50 \times 10^{-3}\ M^{-1}s^{-1}$	[28]
59	$O_3 + OH^- \rightarrow O_2 + HO_2^-$	$7.00 \times 10^1\ M^{-1}s^{-1}$	[29]
60	$O_3 + HO^{\cdot} \rightarrow O_2 + HO_2^{\cdot}$	$1.10 \times 10^8\ M^{-1}s^{-1}$	[29]
61	$O_3 + O_2^{\cdot -} \rightarrow O_3^{\cdot -} + O_2$	$1.60 \times 10^9\ M^{-1}s^{-1}$	[30]
62	$O_3 + HO_2^- \rightarrow O_2 + HO^{\cdot} + O_2^{\cdot -}$	$2.80 \times 10^6\ M^{-1}s^{-1}$	[28]
63	$O_3 + Cl^- \rightarrow O_2 + OCl^-$	$3.00 \times 10^{-3}\ M^{-1}s^{-1}$	[31]
64	$O_3 + HOCl \rightarrow$ Products	$2.00 \times 10^{-3}\ M^{-1}s^{-1}$	[31]
65	$O_3 + OCl^- \rightarrow$ Products	$1.20 \times 10^2\ M^{-1}s^{-1}$	[31]

66	$O_3 + ClO_3^- \rightarrow$ Products	1.00×10^{-4} $M^{-1}s^{-1}$	[31]
67	$O_3 + ClO_4^- \rightarrow$ Products	2.00×10^{-5} $M^{-1}s^{-1}$	[31]
68	$O_3 + Cl_2{\cdot}^- \rightarrow$ Products	9.00×10^{7} $M^{-1}s^{-1}$	[32]
69	$O_3 \rightarrow$ Products	$7.04/3.28 \times 10^{-3}$ s^{-1}	Fitted[d]
70	$O_3{\cdot}^- + H^+ \rightarrow HO_3{\cdot}$	5.20×10^{10} $M^{-1}s^{-1}$	[30]
71	$O_3{\cdot}^- + HO{\cdot} \rightarrow HO_2{\cdot} + O_2{\cdot}^-$	8.50×10^{9} $M^{-1}s^{-1}$	[33]
72	$O_3{\cdot}^- + O{\cdot}^- \rightarrow 2O_2{\cdot}^-$	7.00×10^{8} $M^{-1}s^{-1}$	[34]
73	$O_3{\cdot}^- \rightarrow O_2 + O{\cdot}^-$	3.30×10^{3} s^{-1}	[35]
74	$O_2{\cdot}^- + H_2O_2 \rightarrow O_2 + HO{\cdot} + OH^-$	1.30×10^{-1} $M^{-1}s^{-1}$	[36]
75	$O_2{\cdot}^- + H^+ \rightarrow HO_2{\cdot}$	7.20×10^{10} $M^{-1}s^{-1}$	[37]
76	$O_2{\cdot}^- + HO{\cdot} \rightarrow O_2 + OH^-$	7.00×10^{9} $M^{-1}s^{-1}$	[36]
77	$O_2{\cdot}^- + O{\cdot}^- + H_2O \rightarrow O_2 + 2OH^-$	6.00×10^{8} $M^{-2}s^{-1}$	[34]
78	$O_2{\cdot}^- + HO_2{\cdot} \rightarrow HO_2^- + O_2$	9.70×10^{7} $M^{-1}s^{-1}$	[36]
79	$O_2{\cdot}^- + Cl_2{\cdot}^- \rightarrow O_2 + 2Cl^-$	2.00×10^{9} $M^{-1}s^{-1}$	[20]
80	$O_2{\cdot}^- + Cl^- \rightarrow$ Products	1.40×10^{-2} $M^{-1}s^{-1}$	[38]
81	$O_2{\cdot}^- + HOCl \rightarrow O_2 + Cl^- + HO{\cdot}$	7.50×10^{6} $M^{-1}s^{-1}$	[38]
82	$O{\cdot}^- + O_2 \rightarrow O_3{\cdot}^-$	3.60×10^{9} $M^{-1}s^{-1}$	[10]
83	$O{\cdot}^- + H_2O \rightarrow HO{\cdot} + OH^-$	1.70×10^{6} $M^{-1}s^{-1}$	[10]
84	$O{\cdot}^- + HO{\cdot} \rightarrow HO_2^-$	2.00×10^{10} $M^{-1}s^{-1}$	[10]
85	$O{\cdot}^- + HO_2^- \rightarrow OH^- + O_2{\cdot}^-$	4.00×10^{8} $M^{-1}s^{-1}$	[10]
86	$O{\cdot}^- + OCl^- \rightarrow OCl{\cdot} + OH^-$	2.30×10^{8} $M^{-1}s^{-1}$	[10]
87	$HO_2{\cdot} + H_2O + O_2{\cdot}^- \rightarrow O_2 + H_2O_2 + OH^-$	9.70×10^{7} $M^{-2}s^{-1}$	[38]
88	$HO_2{\cdot} + H_2O_2 \rightarrow O_2 + H_2O + HO{\cdot}$	3.00×10^{0} $M^{-1}s^{-1}$	[36]
89	$HO_2{\cdot} + HO{\cdot} \rightarrow O_2 + H_2O$	6.60×10^{9} $M^{-1}s^{-1}$	[36]
90	$HO_2{\cdot} + HO_2{\cdot} \rightarrow O_2 + H_2O_2$	8.30×10^{5} $M^{-1}s^{-1}$	[36]
91	$HO_2{\cdot} + Cl_2{\cdot}^- \rightarrow O_2 + 2Cl^- + H^+$	3.00×10^{9} $M^{-1}s^{-1}$	[20]
92	$HO_2{\cdot} + Cl_2 \rightarrow Cl_2{\cdot}^- + O_2 + H^+$	1.00×10^{9} $M^{-1}s^{-1}$	[24]
93	$HO_2{\cdot} \rightarrow H^+ + O_2{\cdot}^-$	7.90×10^{5} s^{-1}	[12]

94	$HO_2^- + HO\cdot \rightarrow HO_2\cdot + OH^-$	$7.50 \times 10^9\ M^{-1}s^{-1}$	[10]
95	$HO_3\cdot \rightarrow HO\cdot + O_2$	$1.10 \times 10^5\ s^{-1}$	[30]
96	$HO_3\cdot \rightarrow O_3\cdot^- + H^+$	$3.70 \times 10^4\ s^{-1}$	[30]
97	$BA + HO\cdot \rightarrow P1$	$4.30 \times 10^9\ M^{-1}s^{-1}$	[10]
98	$BA + O\cdot^- \rightarrow P2$	$4.00 \times 10^7\ M^{-1}s^{-1}$	[10]
99	$BA + Cl\cdot \rightarrow P3$	$1.80 \times 10^{10}\ M^{-1}s^{-1}$	[39]
100	$BA + Cl_2\cdot^- \rightarrow P4$	$2.00 \times 10^6\ M^{-1}s^{-1}$	[40]
101	$P1 + O_3 \rightarrow P5 + O_3\cdot^-$	$1.00 \times 10^5\ M^{-1}s^{-1}$	Assumed[e]
102	$P5 + 3O_3 \rightarrow P6 + O_3\cdot^-$	Not important[f]	

a. The concentration of active sites MO was set as unity.
b. No significant amounts of ClO_3^- and ClO_4^- were detected through the course of electrolysis experiments. These two reactions were therefore not taken into account in this model.
c. Reaction 20 accounted for unknown HO· quenching pathways in the solution matrix. The rate was set the same as that assumed in Yang *et al.*[41] where a more detailed explanation was provided. It was assumed that the quenching pathways were similar in the two systems. This assumption also enabled easier comparison between NAT/AT and BDD.
d. Reaction 69 was incorporated into the kinetic model to account for the escape of O_3 from the aqueous to the gas phase and depletion of aqueous O3 through unknown transformation pathways in the solution matrix.
e. The actual rate constant between the transient OH-adduct radical (OH-BA, P1) and O_3 is not quantified in this study and needs further investigation. We chose $1.00 \times 10^5\ M^{-1}s^{-1}$ for our model with two considerations: (1) assuming numbers between 1.00×10^3 and $1.00 \times 10^9\ M^{-1}s^{-1}$ did not significantly affect the fitted HO· production rate (reaction 10), probably because $O_3\cdot^-$ formed in this step is limited by the amount and rate of P1 formed, that is, the rate of reaction 97; (2) aqueous O_3 concentrations predicted using rate constants $\geq 1.00 \times 10^5$ matched better to experimentally measured values in the first 5 min. Predicted O_3 concentrations became higher than experimental ones for two potential reasons: (1) excess O_3 got transformed in the bulk electrolyte where the assumption pH =

2 no longer holds, and/or (2) unknown reactions between O_3 and BA degradation products.

f. Changing the rate constant for reaction 102 (proposed in Huang *et al.*[42]) did not affect the fitting outcome. Due to the fact that this reaction involves the product of reaction 101 as well as three O_3 molecules, it is likely not important in yielding $O_3{\cdot}^-$ and thus HO· to facilitate BA degradation.

Table S3. Rate constants estimated by kinetic modeling.

	In $NaClO_4$	**Avg RMSD[a]/R^2**	**In NaCl**	**Avg RMSD/R^2**
r_{O3}	6.92×10^{-7} s^{-1}	0.036/99.4	1.42×10^{-7} s^{-1}	0.045/99.6
$r_{HO\cdot}$[b]	1.69×10^{-6} s^{-1}	3.48/96.8	1.69×10^{-6} s^{-1}	3.48/96.8
$k_{Cl\cdot}$	-	-	1.50×10^{-5} s^{-1}	0.058/99.5
k_{Cl2}	-	-	8.05×10^{-1} s^{-1}	0.057/99.5
$k_{OCl\cdot}$	-	-	3.89×10^{2} s^{-1}	0.057/99.5
k_{69}	7.04×10^{-3} s^{-1}	0.036/99.4	3.28×10^{-3} s^{-1}	0.045/99.6

a. Root-mean-square-deviation (RMSD), a value of 0 indicates a perfect fit.

b. Comparing to a previously reported SbSn/CoTi/Ir anode,[43] NAT/AT showed two-order-of-magnitude higher $r_{HO\cdot}$ and a lot faster benzoic acid (BA) degradation (~70% removal in 30 mM NaCl after 4 h at 25 mA/cm^2 vs. ~100% removal in 30 mM NaCl after 75 min at 10 mA/cm^2) and COD removal from toilet wastewater. The fitted $r_{HO\cdot}$ and $k_{Cl\cdot}$ values were on the same order of magnitude as those fitted for BDD in another study.[41]

Table S4. Carbamazepine transformation products.

Electrolyte	RT (min)	TP m/z (Name)	Major fragment ions m/z	Calculated formula	Mass error (mDa)	Structure	Ref
$NaClO_4$	1.51	251 (BQM)	180.08 208.077	$C_{15}H_{11}N_2O_2$	0.2	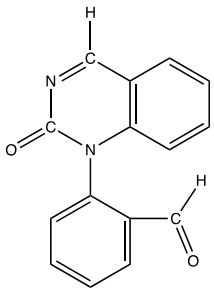	44
NaCl	1.16	180	152.0612	$C_{13}H_{10}N$	0.6	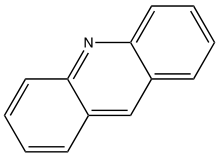	45
	1.51	251 (BQM)	180.08 208.077	$C_{15}H_{11}N_2O_2$	0.5	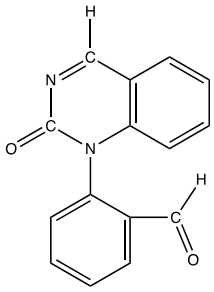	44
	1.59	253	180.0803 210.0912	$C_{15}H_{13}N_2O_2$	0.4	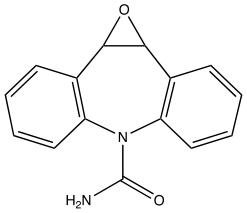	45
	2.09	208	180.0804	$C_{14}H_{10}NO$	0.6	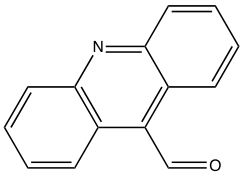	45
	2.43	205	139.9873 141.9825	$C_{14}H_9N_2$	0.6	Structure unknown	

Table S5. Composition of latrine wastewater.

Property	Before EO	After EO (75 min)
pH	8.5-8.8	
Conductivity (mS cm^{-1})	13.3	
COD (mg O_2 L^{-1})	307 ± 13	94 ± 14
[NH_4^+] (mM)	84 ± 6	71 ± 1
[Cl^-] (mM)	65 ± 8	56 ± 3
Average voltage (V)	3.9	

Table S6. Energy consumption for pharmaceuticals/pathogens removal by common electrodes.

Electrode	Solution type[a]	Pharmaceuticals (kWh/m^3)	*E. coli* (kWh/m^3)	MS2 (kWh/m^3)	All (kWh/m^3)
NAT/AT	30 mM $NaClO_4$/NaCl	~0.8 for 1-log removal of 5 pharmaceuticals (10 μM each)	<0.04 for 5-log removal	<0.04 for 5-log removal	~0.8
	Latrine wastewater	~14.0 for 1-log removal of 5 pharmaceuticals (10 μM each)	~3.9 for 5-log removal	<9.4 for 5-log removal	~14.0
Bismuth-doped TiO_2 (Nanopac)	Latrine wastewater[b]	~14.0 for 1-log removal of 8 pharmaceuticals[c] (1 μM each)[45]		2.0 for 5-log removal[46]	
BDD	Secondary effluent		1-4 for 4-log removal[47,48]		
Ti/BDD	2.8 mM Na_2SO_4	>11.3 for >0.3-log removal of 43.2 μM carbamazepine[49]			
Ti/PbO_2	2.8 mM Na_2SO_4	>12.4 for >0.3-log removal of 43.2 μM carbamazepine[49]			
SS/PbO_2	10-120 mM NaCl		0.017 for 3.3-log removal[50]		
Pb/PbO_2	10-120 mM NaCl		0.096 for 3.3-log removal[50]		
Platinum	10-120 mM NaCl		0.11 for 3.3-log removal[50]		
Graphite	10-120 mM NaCl		0.14 for 3.3-log removal[50]		

Platinum clad niobium mesh	30 mM Na_2SO_4	6.3 for 4-log removal[51]	7.8 for 6-log removal[51]

a. While few studies investigated pharmaceutical removal and *E. coli* and MS2 inactivation together, one or two aspects examined in various solutions were selected for comparison purposes. All initial *E. coli* and MS2 concentrations range from 10^4-10^6 CFU or PFU/mL.
b. Toilet wastewater used in these two studies had different compositions than the one used in our experiments, with lower [NH_4^+] and [Cl^-] (<20 and 30 mM comparing to ~84 and 65 mM). By converting free chlorine to chloramines, ammonia can retard disinfection efficiency.
c. The 5 pharmaceuticals used in our study overlapped with the 8 used in this study.

References

(1) Jasper, J. T.; Yang, Y.; Hoffmann, M. R. Toxic Byproduct Formation during Electrochemical Treatment of Latrine Wastewater. *Environ. Sci. Technol.* **2017**, *51* (12), 7111–7119.
(2) Ianni, J. C., *Kintecus*, Windows Version 6.80. www.kintecus.com.
(3) Cho, K.; Hoffmann, M. R. BixTi1–XOz Functionalized Heterojunction Anode with an Enhanced Reactive Chlorine Generation Efficiency in Dilute Aqueous Solutions. *Chem. Mater.* **2015**, *27* (6), 2224–2233.
(4) Chen, X.; Chen, G.; Yue, P. L. Stable Ti/IrOx−Sb2O5−SnO2 Anode for O2 Evolution with Low Ir Content. *J. Phys. Chem. B* **2001**, *105* (20), 4623–4628.
(5) P. Chaplin, B. Critical Review of Electrochemical Advanced Oxidation Processes for Water Treatment Applications. *Environmental Science: Processes & Impacts* **2014**, *16* (6), 1182–1203.
(6) Yang, S. Y.; Kim, D.; Park, H. Shift of the Reactive Species in the Sb–SnO2-Electrocatalyzed Inactivation of E. Coli and Degradation of Phenol: Effects of Nickel Doping and Electrolytes. *Environ. Sci. Technol.* **2014**, *48* (5), 2877–2884.
(7) Cañizares, P.; García-Gómez, J.; Fernández de Marcos, I.; Rodrigo, M. A.; Lobato, J. Measurement of Mass-Transfer Coefficients by an Electrochemical Technique. *J. Chem. Educ.* **2006**, *83* (8), 1204.
(8) Klymenko, O. V.; Evans, R. G.; Hardacre, C.; Svir, I. B.; Compton, R. G. Double Potential Step Chronoamperometry at Microdisk Electrodes: Simulating the Case of Unequal Diffusion Coefficients. *Journal of Electroanalytical Chemistry* **2004**, *571* (2), 211–221.
(9) Noulty, R. A.; Leaist, D. G. Diffusion Coefficient of Aqueous Benzoic Acid at 25.Degree.C. *J. Chem. Eng. Data* **1987**, *32* (4), 418–420.
(10) Buxton, G. V.; Greenstock, C. L.; Helman, W. P.; Ross, A. B. Critical Review of Rate Constants for Reactions of Hydrated Electrons, Hydrogen Atoms and Hydroxyl Radicals (·OH/·O $^-$ in Aqueous Solution. *Journal of Physical and Chemical Reference Data* **1988**, *17* (2), 513–886.

(11) Huber, M. M.; Canonica, S.; Park, G.-Y.; von Gunten, U. Oxidation of Pharmaceuticals during Ozonation and Advanced Oxidation Processes. *Environ. Sci. Technol.* **2003**, *37* (5), 1016–1024.
(12) Yang, Y.; Pignatello, J. J.; Ma, J.; Mitch, W. A. Comparison of Halide Impacts on the Efficiency of Contaminant Degradation by Sulfate and Hydroxyl Radical-Based Advanced Oxidation Processes (AOPs). *Environ. Sci. Technol.* **2014**, *48* (4), 2344–2351.
(13) V. Buxton, G. Pulse Radiolysis of Aqueous Solutions. Rate of Reaction of OH with OH –. *Transactions of the Faraday Society* **1970**, *66* (0), 1656–1660.
(14) G. Jayson, G.; J. Parsons, B.; J. Swallow, A. Some Simple, Highly Reactive, Inorganic Chlorine Derivatives in Aqueous Solution. Their Formation Using Pulses of Radiation and Their Role in the Mechanism of the Fricke Dosimeter. *Journal of the Chemical Society, Faraday Transactions 1: Physical Chemistry in Condensed Phases* **1973**, *69* (0), 1597–1607.
(15) Grigor'ev, A. E.; Makarov, I. E.; Pikaev, A. K. Formation of Cl_2^- in the bulk of solution during radiolysis of concentrated aqueous solutions of chlorides. *Khimiya Vysokikh Ehnergij* **1987**, *21* (2), 123–126.
(16) McElroy, W. John. A Laser Photolysis Study of the Reaction of Sulfate(1-) with Chloride and the Subsequent Decay of Chlorine(1-) in Aqueous Solution. *The Journal of Physical Chemistry* **1990**, *94* (6), 2435–2441.
(17) Yu, X.-Y.; Barker, J. R. Hydrogen Peroxide Photolysis in Acidic Aqueous Solutions Containing Chloride Ions. II. Quantum Yield of HO•(Aq) Radicals. *J. Phys. Chem. A* **2003**, *107* (9), 1325–1332.
(18) Kläning, U. K.; Wolff, T. Laser Flash Photolysis of HClO, ClO−, HBrO, and BrO− in Aqueous Solution. Reactions of Cl- and Br-Atoms. *Berichte der Bunsengesellschaft für physikalische Chemie* **1985**, *89* (3), 243–245.
(19) Nagarajan, V.; Fessenden, R. W. Flash Photolysis of Transient Radicals. 1. X2- with X = Cl, Br, I, and SCN. *The Journal of Physical Chemistry* **1985**, *89* (11), 2330–2335.
(20) Matthew, B. M.; Anastasio, C. A Chemical Probe Technique for the Determination of Reactive Halogen Species in Aqueous Solution: Part 1 ? Bromide Solutions. *Atmospheric Chemistry and Physics Discussions* **2006**, *6* (1), 899–940.
(21) Wu, D.; Wong, D.; Di Bartolo, B. Evolution of Cl−2 in Aqueous NaCl Solutions. *Journal of Photochemistry* **1980**, *14* (4), 303–310.
(22) Wagner, I.; Karthäuser, J.; Strehlow, H. On the Decay of the Dichloride Anion Cl−2 in Aqueous Solution. *Berichte der Bunsengesellschaft für physikalische Chemie* **1986**, *90* (10), 861–867.
(23) Wang, T. X.; Margerum, D. W. Kinetics of Reversible Chlorine Hydrolysis: Temperature Dependence and General-Acid/Base-Assisted Mechanisms. *Inorganic Chemistry* **1994**, *33* (6), 1050–1055.
(24) Bjergbakke, E.; Navaratnam, S.; Parsons, B. J.; Swallow, A. J. Reaction between Hydroperoxo Radicals and Chlorine in Aqueous Solution. *Journal of the American Chemical Society* **1981**, *103* (19), 5926–5928.
(25) Ershov, B. G. Kinetics, Mechanism and Intermediates of Some Radiation-Induced Reactions in Aqueous Solutions. *Russ. Chem. Rev.* **2004**, *73* (1), 101–113.
(26) Connick, R. E. The Interaction of Hydrogen Peroxide and Hypochlorous Acid in Acidic Solutions Containing Chloride Ion. *Journal of the American Chemical Society* **1947**, *69* (6), 1509–1514.

(27) V. Buxton, G.; S. Subhani, M. Radiation Chemistry and Photochemistry of Oxychlorine Ions. Part 1.—Radiolysis of Aqueous Solutions of Hypochlorite and Chlorite Ions. *Journal of the Chemical Society, Faraday Transactions 1: Physical Chemistry in Condensed Phases* **1972**, *68* (0), 947–957.
(28) Staehelin, Johannes.; Hoigne, Juerg. Decomposition of Ozone in Water: Rate of Initiation by Hydroxide Ions and Hydrogen Peroxide. *Environ. Sci. Technol.* **1982**, *16* (10), 676–681.
(29) Lesko, T. M.; Colussi, A. J.; Hoffmann, M. R. Hydrogen Isotope Effects and Mechanism of Aqueous Ozone and Peroxone Decompositions. *J. Am. Chem. Soc.* **2004**, *126* (13), 4432–4436.
(30) Buehler, R. E.; Staehelin, J.; Hoigne, J. Ozone Decomposition in Water Studied by Pulse Radiolysis. 1. Perhydroxyl (HO2)/Hyperoxide (O2-) and HO3/O3- as Intermediates. *J. Phys. Chem.* **1984**, *88* (12), 2560–2564.
(31) Hoigné, J.; Bader, H.; Haag, W. R.; Staehelin, J. Rate Constants of Reactions of Ozone with Organic and Inorganic Compounds in Water—III. Inorganic Compounds and Radicals. *Water Research* **1985**, *19* (8), 993–1004.
(32) Bielski, B. H. J. A Pulse Radiolysis Study of the Reaction of Ozone with Cl÷2 in Aqueous Solutions. *Radiation Physics and Chemistry* **1993**, *41* (3), 527–530.
(33) Sehested, K.; Holcman, J.; Bjergbakke, E.; Hart, E. J. Formation of Ozone in the Reaction of Hydroxyl with O3- and the Decay of the Ozonide Ion Radical at PH 10-13. *The Journal of Physical Chemistry* **1984**, *88* (2), 269–273.
(34) Sehested, K.; Holcman, J.; Bjergbakke, E.; Hart, E. J. Ultraviolet Spectrum and Decay of the Ozonide Ion Radical, O3-, in Strong Alkaline Solution. *The Journal of Physical Chemistry* **1982**, *86* (11), 2066–2069.
(35) Gall, B. L.; Dorfman, L. M. Pulse Radiolysis Studies. XV. Reactivity of the Oxide Radical Ion and of the Ozonide Ion in Aqueous Solution. *Journal of the American Chemical Society* **1969**, *91* (9), 2199–2204.
(36) Crittenden, J. C.; Hu, S.; Hand, D. W.; Green, S. A. A Kinetic Model for H2O2/UV Process in a Completely Mixed Batch Reactor. *Water Research* **1999**, *33* (10), 2315–2328.
(37) Field, R. J.; Noyes, R. M.; Postlethwaite, D. Photoreduction of Hydrogen Peroxide by Hydrogen. *The Journal of Physical Chemistry* **1976**, *80* (3), 223–229.
(38) Bielski, B. H. J.; Cabelli, D. E.; Arudi, R. L.; Ross, A. B. Reactivity of HO2/O−2 Radicals in Aqueous Solution. *Journal of Physical and Chemical Reference Data* **1985**, *14* (4), 1041–1100.
(39) Mártire, D. O.; Rosso, J. A.; Bertolotti, S.; Le Roux, G. C.; Braun, A. M.; Gonzalez, M. C. Kinetic Study of the Reactions of Chlorine Atoms and Cl2•- Radical Anions in Aqueous Solutions. II. Toluene, Benzoic Acid, and Chlorobenzene. *J. Phys. Chem. A* **2001**, *105* (22), 5385–5392.
(40) Hasegawa, K.; Neta, P. Rate Constants and Mechanisms of Reaction of Chloride (Cl2-) Radicals. *J. Phys. Chem.* **1978**, *82* (8), 854–857.
(41) Yang, S.; Fernando, S.; Holsen, T. M.; Yang, Y. Inhibition of Perchlorate Formation during the Electrochemical Oxidation of Perfluoroalkyl Acid in Groundwater. *Environ. Sci. Technol. Lett.* **2019**, *6* (12), 775–780.
(42) Huang, X.; Li, X.; Pan, B.; Li, H.; Zhang, Y.; Xie, B. Self-Enhanced Ozonation of Benzoic Acid at Acidic PHs. *Water Research* **2015**, *73*, 9–16.

(43) Yang, Y.; Shin, J.; Jasper, J. T.; Hoffmann, M. R. Multilayer Heterojunction Anodes for Saline Wastewater Treatment: Design Strategies and Reactive Species Generation Mechanisms. *Environ. Sci. Technol.* **2016**, *50* (16), 8780–8787.
(44) McDowell, D. C.; Huber, M. M.; Wagner, M.; von Gunten, U.; Ternes, T. A. Ozonation of Carbamazepine in Drinking Water: Identification and Kinetic Study of Major Oxidation Products. *Environ. Sci. Technol.* **2005**, *39* (20), 8014–8022.
(45) Jasper, J. T.; Shafaat, O. S.; Hoffmann, M. R. Electrochemical Transformation of Trace Organic Contaminants in Latrine Wastewater. *Environ. Sci. Technol.* **2016**, *50* (18), 10198–10208.
(46) Huang, X.; Qu, Y.; Cid, C. A.; Finke, C.; Hoffmann, M. R.; Lim, K.; Jiang, S. C. Electrochemical Disinfection of Toilet Wastewater Using Wastewater Electrolysis Cell. *Water Research* **2016**, *92*, 164–172.
(47) Schmalz, V.; Dittmar, T.; Haaken, D.; Worch, E. Electrochemical Disinfection of Biologically Treated Wastewater from Small Treatment Systems by Using Boron-Doped Diamond (BDD) Electrodes – Contribution for Direct Reuse of Domestic Wastewater. *Water Research* **2009**, *43* (20), 5260–5266.
(48) Haaken, D.; Dittmar, T.; Schmalz, V.; Worch, E. Influence of Operating Conditions and Wastewater-Specific Parameters on the Electrochemical Bulk Disinfection of Biologically Treated Sewage at Boron-Doped Diamond (BDD) Electrodes. *Desalination and Water Treatment* **2012**, *46* (1–3), 160–167.
(49) García-Gómez, C.; Drogui, P.; Zaviska, F.; Seyhi, B.; Gortáres-Moroyoqui, P.; Buelna, G.; Neira-Sáenz, C.; Estrada-alvarado, M.; Ulloa-Mercado, R. G. Experimental Design Methodology Applied to Electrochemical Oxidation of Carbamazepine Using Ti/PbO2 and Ti/BDD Electrodes. *Journal of Electroanalytical Chemistry* **2014**, *732*, 1–10.
(50) Rahmani, A. R.; Samarghandi, M. R.; Nematollahi, D.; Zamani, F. A Comprehensive Study of Electrochemical Disinfection of Water Using Direct and Indirect Oxidation Processes. *Journal of Environmental Chemical Engineering* **2019**, *7* (1), 102785.
(51) Kerwick, M. I.; Reddy, S. M.; Chamberlain, A. H. L.; Holt, D. M. Electrochemical Disinfection, an Environmentally Acceptable Method of Drinking Water Disinfection? *Electrochimica Acta* **2005**, *50* (25), 5270–5277.